Eur. J. Mineral., 38, 449–459, 2026
https://doi.org/10.5194/ejm-38-449-2026
© Author(s) 2026. This work is distributed under
the Creative Commons Attribution 4.0 License.

European Journal of Mineralogy
Open Access

Xianhuaite-(Ce), $K_2CeNb_5O_{15}$, a new niobium mineral from the Bayan Obo deposit, China

Bo Yang[1,2,3], Yuan Xue[4], Li Yang[3], Ningyue Sun[4], Guowu Li[4], Junfang Yu[1], Guoying Yan[1], Jianyong Liu[1], Yonggang Zhao[5], Wenxiang Meng[1], Zhenyu Chen[6], Lei Chen[4], Ze Liu[6], Zhao Yan[1], Xinyu Hou[1], Xin Ao[1], and Jinlong Wang[1]

[1]Mining Research Institute of Baotou Steel (Group) Corp., Baotou 014030, China
[2]State Key Laboratory of Lithospheric and Environmental Coevolution, Institute of Geology and Geophysics, Chinese Academy of Sciences, Beijing 100029, China
[3]College of Earth and Planetary Sciences, University of Chinese Academy of Sciences, Beijing 100049, China
[4]China University of Geosciences, Beijing 100083, China
[5]Baotou Iron and Steel (Group) Co., Ltd., Baotou 014030, China
[6]Institute of Mineral resources, Chinese Academy of Geological Sciences, Beijing 100037, China

Correspondence: Guowu Li (liguowu@cugb.edu.cn)

Received: 6 March 2026 – Revised: 3 June 2026 – Accepted: 10 June 2026 – Published: 21 July 2026

Abstract. Xianhuaite-(Ce), $K_2CeNb_5O_{15}$, is a new mineral species discovered in the Bayan Obo deposit, Inner Mongolia, China. The mineral is named in honor of Professor Xianhua Li in recognition of his outstanding contributions to research on the Bayan Obo deposit. It occurs as brownish-red to pale yellow-brown tetragonal prisms or irregular granules and exhibits a Mohs hardness of 5–6, an adamantine luster, and a calculated density of 5.23 g cm^{-3}. Electron microprobe analysis yields the empirical formula $^{A1}(K_{1.30}Ba_{0.69}Sr_{0.02})_{\Sigma 2.01}{}^{A2}(Ce_{0.39}La_{0.31}Nd_{0.04}Pr_{0.02}Ca_{0.15}Na_{0.09})_{\Sigma 1.00}{}^{B}(Nb_{4.75}Fe^{3+}_{0.13}Ti_{0.09}Mg_{0.04})_{\Sigma 5.01}O_{15}$. Xianhuaite-(Ce) crystallizes in the tetragonal system, space group $P4/mbm$, with unit-cell parameters $a = 12.5355(4)$ Å, $c = 3.9213(2)$ Å, $V = 616.19(5)$ Å^3, and $Z = 2$. Its crystal structure adopts a tetragonal tungsten bronze (TTB)-type framework, characterized by corner-sharing NbO_6 octahedra forming channels hosting K, Ba, and rare earth element (REE) cations. Xianhuaite-(Ce) is associated with minerals typical of skarnization assemblages (e.g. dolomite, forsterite, phlogopite, and chlorite), as well as other Nb phases, including fersmite, columbite-(Fe), fergusonite-(Ce), and aeschynite. As the first naturally occurring mineral with a TTB-type structure, xianhuaite-(Ce) expands the known structural diversity of Nb minerals and provides new mineralogical constraints on Nb mineralization at Bayan Obo.

1 Introduction

The Bayan Obo deposit in northern China is a world-class rare earth element (REE)–niobium (Nb) deposit (Huang et al., 2024; Li et al., 2025). In addition to hosting the largest known global REE reserves, it contains significant Nb resources (She et al., 2021; Ren et al., 2023; Li et al., 2024; Chen et al., 2025). Owing to the strategic importance of REE and Nb in advanced technological and defense applications (Rooks et al., 2025), the deposit has been the focus of sustained geological and mineralogical research (Institute of Geochemistry, Chinese Academy of Sciences, 1988; Yang et al., 2024a; Yu et al., 2024).

Despite decades of investigation, fundamental mineralogical issues concerning Nb enrichment at Bayan Obo remain unresolved (Institute of Geochemistry, Chinese Academy of Sciences, 1988; Yang et al., 2024a). Nb is distributed among numerous discrete mineral species rather than being concentrated in a single dominant host. To date, at least 30 Nb or Nb-bearing minerals have been identified, reflecting exceptional mineralogical diversity and extensive elemental isomorphism (Yang et al., 2024b). Such complexity obscures

the crystallochemical mechanisms governing Nb incorporation, stabilization, and redistribution, underscoring the necessity of mineral-scale investigations (Yang et al., 2024a; Yu et al., 2024). In particular, Nb or Nb-bearing minerals with previously unrecognized compositional or structural characteristics are critical for constraining the crystallographic controls on Nb mineralization.

Within this context, xianhuaite-(Ce), a compositionally and structurally distinct Nb mineral, provides new insight into Nb mineralization processes. It is the first naturally occurring mineral exhibiting a tetragonal tungsten bronze (TTB)-type structure and has the ideal chemical formula $K_2CeNb_5O_{15}$. The mineral and its name have been approved by the International Mineralogical Association Commission on New Minerals, Nomenclature and Classification (IMA-CNMNC) under proposal number IMA 2024-091.

Xianhuaite-(Ce) is named in honor of Professor Xianhua Li, academician of the Chinese Academy of Sciences, in recognition of his significant contributions to studies of early Earth and planetary evolution and especially to recent advances in the geochronology, geochemistry, and resource development of the Bayan Obo deposit. The approved mineral symbol is Xhu-Ce. The holotype specimen (under catalog no. GMCTM2024012) is deposited in the Geological Museum of China (Xisi Yangrou hutong no. 15, Xicheng District, Beijing), P.R. China. The co-type specimen is deposited at the Crystal Structure Laboratory, China University of Geosciences, Beijing 100083, People's Republic of China, under catalog no. BYEB-3.

2 Occurrence and associated minerals

Xianhuaite-(Ce) was identified in two specimens collected from the East Orebody and the East Contact Zone of the Bayan Obo deposit. Overviews of the geology and mineralogy of the Bayan Obo deposit can be found in the Institute of Geochemistry, Chinese Academy of Sciences (1988), and Yang et al. (2024b), among other publications.

Sample BY-E2024-103 was collected from the East Orebody (coordinates: 41°48′01″ N, 109°59′39″ E). The specimen occurs as black-brown megacrystalline aggregates at the contact between aegirine-type Nb–REE–Fe ore and dolomite-type Nb–REE–Fe ore. Analytical work was conducted on fragments mechanically separated from the sample (Fig. 1a–d). The principal minerals in sample BY-E2024-103 are xianhuaite-(Ce), fersmite, and fergusonite-(Ce) (Fig. 1a–d).

Sample BY-EC2024-14 was collected from the East Contact Zone (coordinates: 41° 48′47″ N, 110° 01′27″ E) and belongs to dolomite-type Nb–REE–Fe ore. After cutting and polishing, the specimen was analyzed using a Tescan integrated mineral analyzer (TIMA) (Fig. 1e–h). Quantitative mineralogical data indicate that the sample is composed of dolomite (71.89 vol %), magnetite (12.19 vol %), fersmite (8.00 vol %), calcite (2.69 vol %), columbite-(Fe) (1.72 vol %), xianhuaite-(Ce) (0.40 vol %), aeschynite (0.37 vol %), fergusonite-(Ce) (0.28 vol %), kinoshitalite (0.21 vol %), pyrochlore (0.19 vol %), phlogopite (0.18 vol %), barite (0.15 vol %), apatite (0.10 vol %), chlorite (0.09 vol %), biotite (0.05 vol %), and forsterite (0.02 vol %), with other minerals accounting for 1.47 vol % (Fig. 1g–h). In this sample, xianhuaite-(Ce) occurs in close spatial association with magnetite, fersmite, columbite-(Fe), and fergusonite-(Ce), forming mineral aggregates (Fig. 1g–h). Anhedral pyrochlore grains are commonly preserved as inclusions within both fersmite and xianhuaite-(Ce) (Fig. 1e–f).

3 Physical and optical properties

Xianhuaite-(Ce) occurs as irregular grains or tetragonal prisms ranging in size from $0.03 \times 0.03 \times 0.1$ to $0.4 \times 0.4 \times 0.6$ mm. In hand specimens the mineral is dark brown to black brown, whereas thin fragments appear pale yellow brown to brownish red in transmitted light (Fig. 1a–b), with a white streak and adamantine luster. No fluorescence is observed under longwave (365 nm) ultraviolet radiation. The mineral has a Mohs hardness of 5–6 (measured using a Mohs hardness test pen) and a micro-indentation hardness of 469.5 (mean) with a range of 448.7–490.2 kg mm^{-2} (VHN, 200 g load). It displays perfect cleavage on {001} (Fig. 1b), with no parting observed, and is brittle in tenacity, showing a conchoidal fracture. The calculated density, based on the empirical formula and unit-cell volume refined from single-crystal XRD data, is 5.23 g cm^{-3}. Magnetic properties are none.

This translucent mineral has a calculated refractive index (N_{calc}) of 2.22 (determined by $N = Kd + 1$, with K values from Mandarino, 1981). Reflectivity ranges from R_{min}–R_{max}: 17.6–18.5 (470 nm), 17.4–18.5 (546 nm), 17.3–18.3 (589 nm), and 17.2–18.4 (650 nm). The reflectance values for xianhuaite-(Ce) were measured in air using a CRAIC 20/30PV Pro microspectrophotometer at Westlake University (Hangzhou, China), with aluminum metal ($R = 90$ %) as the reference material. Data were collected from six spots across six grains (×50 objective, 5 × 5 µm aperture), and reflectance results are shown in Fig. 2. In reflected light, the mineral appears grey.

4 Chemical composition

Electron probe microanalysis (EPMA) with wavelength-dispersive spectrometry (WDS) was performed using a JXA-iHP200F electron probe microanalyzer at the Institute of Mineral Resources, Chinese Academy of Geological Sciences. Analytical conditions were 15 kV accelerating voltage, 20 nA beam current, and 10 spot analyses on a single grain. Backscattered electron imaging (Fig. 1e) confirms the

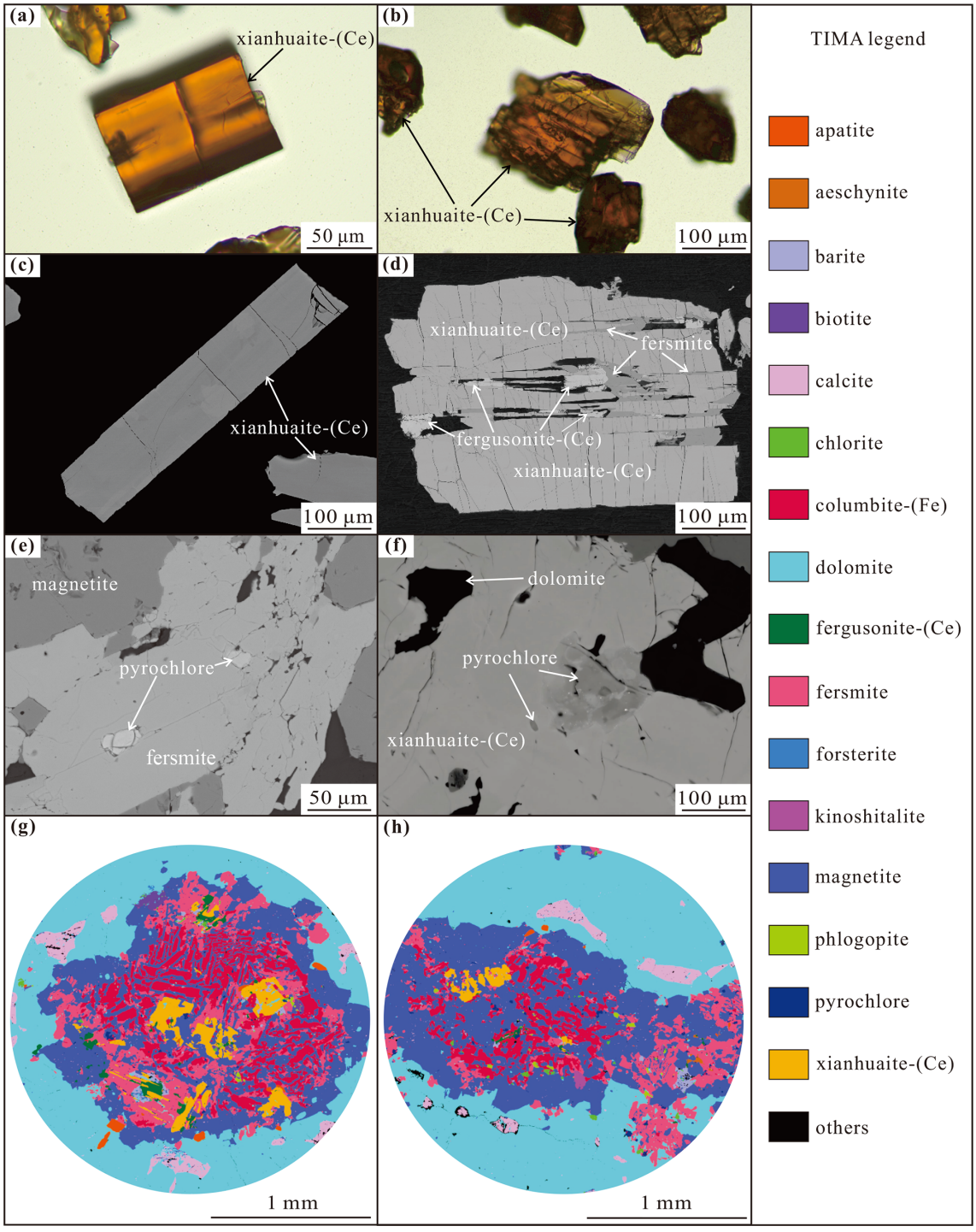

Figure 1. Transmitted-light photomicrographs, backscattered electron (BSE) images, and TIMA false-color mineral maps of samples. **(a)** Euhedral xianhuaite-(Ce) crystals observed under transmitted light in sample BY-E2024-103. **(b)** Well-developed cleavage sets in xianhuaite-(Ce) from sample BY-E2024-103 (transmitted light). **(c–d)** Euhedral grains of xianhuaite-(Ce) and associated minerals in sample BY-E2024-103 (BSE). **(e–f)** Relict pyrochlore enclosed within fersmite and xianhuaite-(Ce) in sample BY-EC2024-14 (BSE). **(g–h)** TIMA false-color mineral maps illustrating the spatial distribution of xianhuaite-(Ce) and its paragenetic associations with other minerals in sample BY-EC2024-14.

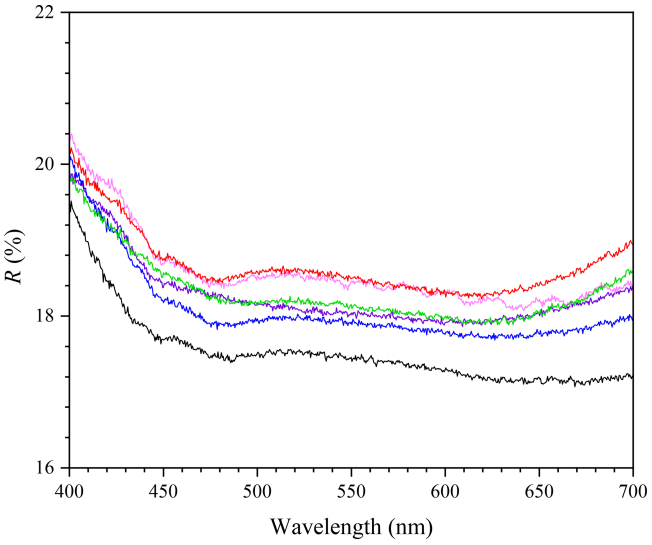

Figure 2. Reflectance data (R, %) for xianhuaite-(Ce) in air, plotted versus wavelength in nm.

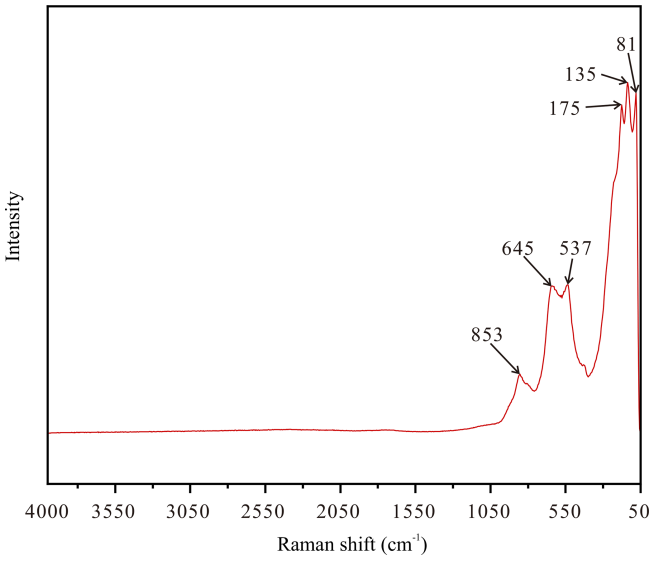

Figure 3. Raman spectrum of xianhuaite-(Ce).

Table 1. Chemical data (in wt %) of xianhuaite-(Ce).

Constituent	Mean	Range	SD (σ)	Reference Material
Nb_2O_5	65.45	64.38–66.47	0.65	$KNbO_3$
BaO	11.19	8.96–12.28	1.02	Barite
Ce_2O_3	6.65	6.33–7.07	0.28	H_2CeO_5P
K_2O	6.28	5.97–7.03	0.32	$KNbO_3$
La_2O_3	5.26	4.78–5.82	0.32	H_2LaO_5P
Fe_2O_3	1.18	0.67–1.74	0.33	Magnetite
CaO	0.91	0.67–1.13	0.14	Apatite
Nd_2O_3	0.75	0.63–0.83	0.07	H_2NdO_5P
TiO_2	0.63	0.44–1.21	0.25	Rutile
Pr_2O_3	0.28	0.00–0.23	0.14	H_2PrO_5P
Ta_2O_5	0.08	0.00–0.20	0.09	$LiTaO_3$
Na_2O	0.31	0.26–0.35	0.02	Jadeite
MgO	0.17	0.09–0.27	0.06	Forsterite
SrO	0.16	0.09–0.23	0.04	Celestite
Total	99.30			

chemical homogeneity at the micrometer scale. Elemental contents and their variation ranges are detailed in Table 1.

Calculated based on oxygen (O) = 15 atoms per formula unit (apfu), the empirical formula of xianhuaite-(Ce) is $^{A1}(K_{1.30}Ba_{0.69}Sr_{0.02})_{\Sigma 2.01}{}^{A2}(Ce_{0.39}La_{0.31}Nd_{0.04}Pr_{0.02}Ca_{0.15}Na_{0.09})_{\Sigma 1.00}{}^{B}(Nb_{4.75}Fe^{3+}_{0.13}Ti_{0.09}Mg_{0.04})_{\Sigma 5.01}O_{15}$. The simplified formula is $(K,Ba)_2(Ce,La)(Nb,Fe)_5O_{15}$, and the further refined ideal formula is $K_2CeNb_5O_{15}$. For this ideal formula, the corresponding oxide composition and weight percentages are Nb_2O_5 72.01, Ce_2O_3 17.78, and K_2O 10.21, with a total of 100 wt %.

5 Raman spectroscopy

Raman measurements were performed using a WITec 300R spectrometer in reflection mode at the Institute of Geology and Geophysics, Chinese Academy of Sciences (IGGCAS), equipped with a 300 line mm^{-1} grating and laser excitation at 532 nm. Spectral data were acquired over the 50–4000 cm^{-1} range with a 45 s collection time, 20 scans, and 0.5 cm^{-1} resolution.

The Raman spectrum of xianhuaite-(Ce) (Fig. 3) exhibits characteristic vibrational modes diagnostic of the TTB-type structure. A prominent band centered at $\sim$ 853 cm^{-1} is assigned to NbO_6 octahedral vibrations. Additional peaks at 645 and 537 cm^{-1} correspond to Nb–O stretching vibrations within the NbO_6 octahedra. In the low-frequency region, a peak at 175 cm^{-1} is attributed to internal NbO_6 modes, while external modes at 135 and 81 cm^{-1} are typical of cation motions in the tetragonal phase of TTB-type structures (Amira et al., 2010). No peaks are observed above 1000 cm^{-1}.

6 Crystallography

6.1 X-ray powder diffraction

X-ray powder diffraction measurements were performed using a Rigaku XtaLAB PRO-007HF diffractometer operated in crystal rotation mode at the China University of Geosciences. The instrument was configured with a rotating anode microfocus X-ray source (Mo$K\alpha$ radiation, $\lambda = 0.71073$ Å), generating 50 kV and 24 mA, coupled to a hybrid pixel array detector for signal acquisition. Collected powder patterns were processed to refine unit-cell parameters via Chekcell software. Simulated diffraction patterns, calculated based on the refined structure, were generated us-

ing VESTA (Momma and Izumi, 2011) to facilitate phase identification and comparison.

X-ray powder diffraction data of xianhuaite-(Ce) are presented in Table 2. There is a good match between the observed and calculated powder diffraction patterns. The unit-cell parameters refined from the powder-diffraction data are $a = 12.5458(8)$ Å, $c = 3.9279(1)$ Å, and $V = 618.24(9)$ Å^3.

6.2 Single-crystal X-ray diffraction

Single-crystal X-ray diffraction data were collected using the same Rigaku XtaLAB PRO-007HF diffractometer to maintain methodological consistency. A euhedral crystal fragment ($0.02 \times 0.02 \times 0.01$ mm) was selected for analysis, with data collection covering a hemispherical reciprocal space region defined by $-15 \le h \le 17$, $-16 \le k \le 16$, and $-5 \le l \le 5$. Raw intensity data underwent Lorentz-polarization correction and multi-scan absorption correction to minimize systematic errors. Structure determination was initiated with SHELXT (Sheldrick, 2015), followed by full-matrix least-squares refinement of atomic coordinates and displacement parameters using OLEX2-1.3 (Dolomanov et al., 2010).

The unit-cell parameters obtained from single-crystal XRD data are as follows: $a = 12.5355$ (4) Å, $c = 3.9213$ (2) Å, and $V = 616.19$ (5) Å^3. The crystal structure is described within the space group $P4/mbm$ (#127). The structure was refined to $R_1 = 0.0189$ based on 427 independent reflections with $I > 2\sigma_I$. A summary of the details for data collection and refinement procedures can be found in Table 3. Atom coordinates, site occupancies, and bond lengths are given in Tables 4–6. The bond valence sum (BVS) calculation is shown in Table 7. The crystal structure data of the xianhuaite-(Ce) is available in the Online Materials CIF file.

Xianhuaite-(Ce) exhibits a tetragonal tungsten bronze (TTB)-type structure (Fig. 4), with NbO_6 octahedra constituting the fundamental framework. These octahedra share corners, creating a tunnel structure along the c axis. In the ab plane, the octahedra interconnect to form a two-dimensional network, generating four-membered and five-membered NbO_6 octahedra rings that provide channels for accommodating cations (Fig. 4a). The channels formed by the five-membered rings are slightly larger and, in xianhuaite-(Ce), host K and Ba cations. The channels formed by the four-membered rings accommodate REE and Ca cations. These large cations are distributed between the network layers in the ab plane, stabilizing the structure (Fig. 4b).

1. $A1$ sites: The $A1$ sites in the xianhuaite-(Ce) structure, which are identified as the largest cation positions within the channels composed of five-membered rings, are occupied by K and Ba ions, with a coordination number of 9. The bond lengths range from 2.80 to 3.19 Å. Structural refinement results indicate an occupancy of $K_{0.642(3)}Ba_{0.358(3)}$ at the $A1$ sites.

2. $A2$ sites: The $A2$ sites, identified as the cation positions within the channels composed of four-membered rings, are primarily occupied by REE and Ca, with a coordination number of 12 and bond lengths ranging from 2.64 to 2.70 Å. Structural refinement results indicate an occupancy of $^{REE}Ce_{0.812(4)}Ca_{0.188(4)}$ at this position.

3. B sites: The B sites are octahedrally coordinated positions, further divided into two crystallographically independent sites, $B1$ and $B2$, both predominantly occupied by Nb. The atom at the $B1$ site exhibits a slightly higher atomic displacement parameter than that at the $B2$ site, suggesting potential minor isomorphic substitution by lighter elements. During structural refinement, a small amount of Fe substitution was modeled at the $B1$ site, resulting in an occupancy of $Nb_{0.947(15)}Fe_{0.053(15)}$, which is also supported by the chemical composition analysis. The bond lengths at the $B1$ site closely approximate those of an ideal octahedron, with bond lengths ranging from 1.96 to 1.97 Å and an average bond length of 1.964 Å. The $B2$ octahedron shows slight distortion, with bond lengths ranging from 1.89 to 2.03 Å and an average bond length of 1.975 Å.

7 Discussion and conclusions

7.1 Genesis of xianhuaite-(Ce)

The Bayan Obo deposit has undergone a complex, multi-stage geological evolution, resulting in exceptional diversity of Nb and Nb-bearing mineral assemblages (Yang et al., 2023; Yang et al., 2024b). Despite decades of investigation, the mechanisms of Nb mineralization remain highly debated (Yang et al., 2024c; Yu et al., 2024), largely because Nb is distributed among numerous discrete mineral phases rather than being concentrated in a single dominant host. Consequently, elucidating the formation conditions of individual Nb and Nb-bearing minerals is essential for constraining the processes responsible for Nb enrichment. In this context, the occurrence of the new mineral xianhuaite-(Ce) in both the East Orebody (BY-E2024-103) and the East Contact Zone (BY-EC2024-14) provides additional constraints on Nb mineralization at the Bayan Obo deposit.

In sample BY-EC2024-14, Nb minerals such as xianhuaite-(Ce), fersmite, and columbite-(Fe) predominantly occur as interstitial phases between magnetite grains (Fig. 1g–h). In addition, both xianhuaite-(Ce) and fersmite contain relict pyrochlore (Fig. 1e–f), indicating inheritance from an earlier Nb mineralization stage. These textural relationships are inconsistent with primary magmatic crystallization and instead suggest precipitation from Nb-bearing fluids during a later hydrothermal overprint. This interpretation is further supported by petrographic evidence for skarn-type alteration in sample BY-EC2024-14, where the assemblage of forsterite, phlogopite, chlorite,

Table 2. X-ray powder diffraction data (d in Å, intensity is I/I_0) for xianhuaite-(Ce).

I_{obs}	d_{obs}	d_{cal}	I_{cal}	hkl
20	8.91	8.8639	19	1 1 0
16	6.26	6.2678	14	2 0 0
25	**3.915**	3.9213	20	0 0 1
11	3.582	3.5861	9	1 1 1
28	**3.469**	3.4767	38	3 2 0
61	**3.208**	3.2132	59	2 1 1
11	3.120	3.1339	16	4 0 0
53	**3.034**	3.0403	67	4 1 0
40	**2.931**	2.9546, 2.9368	5, 36	3 3 0, 2 2 1
100	**2.785**	2.8030, 2.7878	45, 100	4 2 0, 3 1 1
24	2.595	2.6015	22	3 2 1
3	2.322	2.3278	6	5 2 0
9	2.145	2.1498	18	5 3 0
4	2.084	2.0893, 2.0829	3, 4	6 0 0, 5 1 1
44	**1.960**	1.9820, 1.9607, 1.9292	20, 36, 4	6 2 0, 0 0 2, 4 4 1
15	1.868	1.8851, 1.8687, 1.8439	7, 15, 18	5 3 1, 6 3 0, 6 0 1
14	1.771	1.7728, 1.7728, 1.7689, 1.7516	6, 8, 7, 18	5 5 0, 7 1 0, 6 2 1, 5 4 1
6	1.710	1.7078	9	3 2 2
3	1.687	1.6869	13	6 3 1
12	1.649	1.6622, 1.6477	5, 23	4 0 2, 4 1 2
21	1.612	1.6154, 1.6154, 1.6066	28, 13, 18	7 1 1, 5 5 1, 4 2 2
9	1.520	1.5202, 1.5177	11, 3	8 2 0, 7 3 1
3	1.468	1.4773, 1.4672	7, 7	6 6 0, 8 3 0
5	1.449	1.4487	10	5 3 2
3	1.394	1.3939	10	6 2 2
3	1.374	1.3741	7	8 3 1
5	1.354	1.3660, 1.3527	4, 8	7 5 1, 6 3 2
6	1.317	1.3150, 1.3149	4, 4	5 5 2, 7 1 2
5	1.274	1.273	3	2 1 3
5	1.255	1.2414	7	3 1 3
9	1.202	1.2014	9	8 2 2
3	1.191	1.1886	6	10 1 1
4	1.180	1.1799, 1.1747	5, 5	6 6 2, 8 3 2
6	1.163	1.1628	12	9 5 1
4	1.109	1.1081	3	6 0 3
3	1.090	1.0902	3	11 1 1
3	1.058	1.0586, 1.0586	4, 4	9 7 1, 11 3 1
4	1.052	1.0521	5	7 1 3
6	0.891	0.8909	4	9 5 3
4	0.842	0.8435	3	12 6 2

Lines with $I/I_0 \geq 3$ are listed, and the seven strongest observed lines are in bold.

and dolomite is characteristic of magnesian skarn systems typically formed by metasomatism associated with granite intrusion into dolomitic host rocks (Mazurov et al., 2018).

The East Contact Zone is known to have experienced variable degrees of skarnization during emplacement of Permian granites (Yang et al., 2024c). Although this thermal event did not introduce new Nb into the system, it likely facilitated remobilization of pre-existing Nb (Yang et al., 2024c). Taken together, the mineral assemblages, textural relationships, and regional geological context suggest that xianhuaite-(Ce) most plausibly formed under fluid-dominated conditions during the Permian granitic thermal event, thereby recording Nb remobilization and redistribution rather than primary Nb accumulation.

Sample BY-E2024-103 is coarse-grained and lacks diagnostic mineral assemblages that would allow direct petrographic constraints on its formation. However, regional geochronological data indicate that the Permian thermal event affected the entire Bayan Obo district (Institute of Geochemistry, Chinese Academy of Sciences, 1988; Yang et al., 2024c; Yu et al., 2024; Yao et al., 2025). On this basis, xianhuaite-(Ce) in BY-E2024-103 is tentatively interpreted

Table 3. Information on crystal and structural refinement for xianhuaite-(Ce).

Crystal data	
Chemical formula from SREF	$K_{1.285}Ba_{0.715}Ce_{0.812}Ca_{0.188}Nb_{4.947}Fe_{0.053}O_{15}$
M_r	972.07
Crystal system, space group	Tetragonal, $P4/mbm$
Temperature (K)	293
a, c (Å)	12.5355(4), 3.9213(2)
V (Å^3)	616.19(5)
Z	2
Radiation type	Mo$K\alpha$
μ (mm^{-1})	10.28
Crystal size (mm)	0.02 × 0.02 × 0.01
Data collection	
Diffractometer	XtaLAB PRO-007HF
Absorption correction	Multi-scan
T_{min}, T_{max}	0.809, 1.000
No. of measured, independent, and observed [$I>2\sigma_I$] reflections	4897, 480, 427
R_{int}	0.036
(sin $\theta/\lambda)_{max}$ (Å^{-1})	0.687
Refinement	
$R[F^2>2\sigma(F^2)]$, $wR(F^2)$, S	0.0189, 0.042, 1.11
No. of reflections	480
No. of parameters	44
$\Delta\rho_{max}$, $\Delta\rho_{min}$ (e Å^{-3})	0.65, −1.31

Table 4. Site, Wyckoff position (Wyck.), site occupancy, fractional atomic coordinates, and equivalent isotropic displacement parameters (Å^2) of atoms for xianhuaite-(Ce).

Site	Atom	Wyck.	Occupancy	x/a	y/b	z/c	U_{eq}
*A*1	K	4*g*	0.642 (3)	0.32844 (5)	0.17156 (5)	0.000000	0.0198 (3)
	Ba	4*g*	0.358 (3)	0.32844 (5)	0.17156 (5)	0.000000	0.0198 (3)
*A*2	Ce	2*a*	0.812 (4)	0.500000	0.500000	1.000000	0.0083 (2)
	Ca	2*a*	0.188 (4)	0.500000	0.500000	1.000000	0.0083 (2)
*B*1	Nb1	2*c*	0.947 (15)	0.000000	0.500000	0.500000	0.0193 (4)
	Fe1	2*c*	0.053 (15)	0.000000	0.500000	0.500000	0.0193 (4)
*B*2	Nb2	8*j*	1.00	0.28547 (3)	0.42537 (3)	0.500000	0.00760 (14)
	O1	2*d*	1.00	0.000000	0.500000	0.000000	0.036 (2)
	O2	8*j*	1.00	0.1568 (3)	0.5040 (3)	0.500000	0.0205 (8)
	O3	4*h*	1.00	0.2159 (3)	0.2841 (3)	0.500000	0.0116 (10)
	O4	8*i*	1.00	0.3032 (4)	0.4250 (4)	1.000000	0.0358 (12)
	O5	8*j*	1.00	0.3667 (3)	0.5638 (3)	0.500000	0.0265 (10)

Table 5. Anisotropic displacement parameters (in Å^2) for xianhuaite-(Ce).

Site	Atom	U^{11}	U^{22}	U^{33}	U^{12}	U^{13}	U^{23}
*A*1	K	0.0235 (4)	0.0235 (4)	0.0123 (4)	0.0126 (4)	0.000	0.000
	Ba	0.0235 (4)	0.0235 (4)	0.0123 (4)	0.0126 (4)	0.000	0.000
*A*2	Ce	0.0081 (2)	0.0081 (2)	0.0087 (3)	0.000	0.000	0.000
	Ca	0.0081 (2)	0.0081 (2)	0.0087 (3)	0.000	0.000	0.000
*B*1	Nb1	0.0091 (4)	0.0091 (4)	0.0397 (7)	−0.0006 (4)	0.000	0.000
	Fe1	0.0091 (4)	0.0091 (4)	0.0397 (7)	–0.0006 (4)	0.000	0.000
*B*2	Nb2	0.0059 (2)	0.0077 (2)	0.0092 (2)	−0.00017 (15)	0.000	0.000
	O1	0.047 (3)	0.047 (3)	0.014 (4)	−0.015 (5)	0.000	0.000
	O2	0.0066 (15)	0.0085 (15)	0.047 (2)	0.0036 (16)	0.000	0.000
	O3	0.0061 (14)	0.0061 (14)	0.023 (3)	−0.0013 (18)	0.000	0.000
	O4	0.030 (2)	0.070 (3)	0.0069 (19)	−0.022 (2)	0.000	0.000
	O5	0.021 (2)	0.0085 (17)	0.050 (3)	−0.0063 (16)	0.000	0.000

Table 6. Selected geometric parameters (Å) for xianhuaite-(Ce). The bold font indicates the mean bond lengths.

K|Ba–O1^{i}	3.0415 (8)	Ce|Ca–O4^{i}	2.641 (4)
K|Ba–O2^{ii}	2.879 (3)	Ce|Ca–O4^{vii}	2.641 (4)
K|Ba–O2^{iii}	2.879 (3)	Ce|Ca–O4^{viii}	2.641 (4)
K|Ba–O2^{i}	2.879 (3)	Ce|Ca–O4	2.641 (4)
K|Ba–O2^{iv}	2.879 (3)	Ce|Ca–O5^{i}	2.697 (3)
K|Ba–O3^{v}	2.797 (3)	Ce|Ca–O5^{ix}	2.697 (3)
K|Ba–O3	2.797 (3)	Ce|Ca–O5^{x}	2.697 (3)
K|Ba–O4^{v}	3.193 (5)	Ce|Ca–O5^{viii}	2.697 (3)
K|Ba–O4^{vi}	3.193 (5)	Ce|Ca–O5^{xi}	2.697 (3)
< **K|Ba–O**>	**2.949**	Ce|Ca–O5^{xii}	2.697 (3)
		Ce|Ca–O5	2.697 (3)
		Ce|Ca–O5^{vii}	2.697 (3)
		< **Ce|Ca–O**>	**2.678**
Nb1|Fe1–O1	1.9607 (1)	Nb2–O2	1.890 (3)
Nb1|Fe1–O1^{xii}	1.9607 (1)	Nb2–O3	1.9743 (15)
Nb1|Fe1–O2	1.966 (3)	Nb2–O4	1.9732 (5)
Nb1|Fe1–O2^{xiii}	1.966 (3)	Nb2–O4^{v}	1.9732 (5)
Nb1|Fe1–O2^{xiv}	1.966 (3)	Nb2–O5	2.012 (3)
Nb1|Fe1–O2^{xv}	1.966 (3)	Nb2–O5^{i}	2.027 (3)
< **Nb1|Fe1–O**>	**1.964**	<**Nb2–O**>	**1.975**

Symmetry codes: (i) $-y+1, x, z$; (ii) $-x+1/2, y-1/2, -z$; (iii) $-x+1/2, y-1/2, -z+1$; (iv) $-y+1, x, z-1$; (v) $x, y, z-1$; (vi) $-y+1/2, -x+1/2, z-1$; (vii) $-x+1, -y+1, -z+2$; (viii) $y, -x+1, -z+2$; (ix) $-x+1, -y+1, -z+1$; (x) $-y+1, x, z+1$; (xi) $y, -x+1, -z+1$; (xii) $x, y, z+1$; (xiii) $-x, -y+1, -z+1$; (xiv) $y-1/2, x+1/2, -z+1$; (xv) $-y+1/2, -x+1/2, z$; (xvi) $-y, x, z$; (xvii) $y, -x+1, -z$; and (xviii) $x, y, -z+2$.

as having formed during the same Permian Nb remobilization event, although direct geochronological constraints are presently lacking.

7.2 Structural significance and comparison with synthetic analogues

Xianhuaite-(Ce), ideally $K_2CeNb_5O_{15}$, has a synthetic analogue with the same ideal composition and belongs to the tetragonal tungsten bronze (TTB)-type structural family. Zeng et al. (2024) reported that this TTB-type series may undergo temperature-dependent transitions from *P*4*bm* to

Table 7. Bond valence sums for xianhuaite-(Ce).

Atom	K|Ba	Ce|Ca	Nb1|Fe1	Nb2	O Sum
O1	0.10 $^{\times1\downarrow\times2\rightarrow}$		0.87 $^{\times2\downarrow\times2\rightarrow}$		1.94
O2	0.15 $^{\times4\downarrow\times2\rightarrow}$		0.86 $^{\times4\downarrow\times1\rightarrow}$	1.07 $^{\times1\downarrow\times1\rightarrow}$	2.23
O3	0.18 $^{\times2\downarrow\times2\rightarrow}$			0.86 $^{\times1\downarrow\times2\rightarrow}$	2.08
O4	0.07 $^{\times2\downarrow\times1\rightarrow}$	0.24 $^{\times4\downarrow\times1\rightarrow}$		0.86 $^{\times2\downarrow\times2\rightarrow}$	2.02
O5		0.21 $^{\times8\downarrow\times2\rightarrow}$		0.77 $^{\times1\downarrow\times1\rightarrow}$ 0.74 $^{\times1\downarrow\times1\rightarrow}$	1.93
Sum	1.21	2.63	5.17	5.15	

Note: the BVS was calculated from the bond valences using the ECoN21 program (Ilinca, 2022). Site occupancy – *A*1 site, $K^{+}_{0.642}Ba^{2+}_{0.358}$; *A*2 site, $Ce_{0.812}Ca_{0.188}$; *B*1 site, $Nb_{0.947}Fe_{0.053}$; *B*2 site, $Nb_{1.00}$. The bond valence parameters of K^{+}–O^{2-}, Ba^{2+}–O^{2-}, Ca^{2+}–O^{2-}, Ce^{3+}–O^{2-}, and Fe^{3+}–O^{2-} are from Gagné and Hawthorne (2015), and those of Nb^{5+}–O^{2-} are from Tytko et al. (1999).

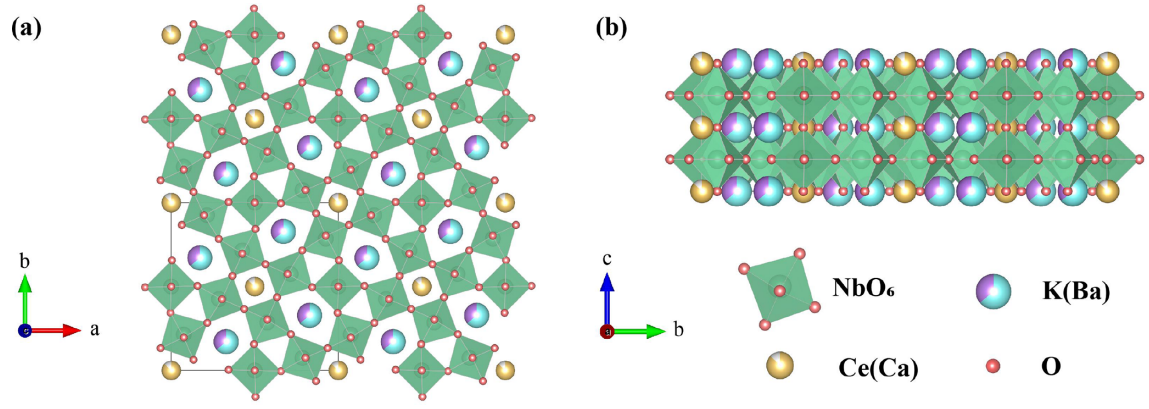

Figure 4. The tetragonal tungsten bronze (TTB)-type structure of xianhuaite-(Ce). **(a)** Two-dimensional network of corner-sharing NbO_6 octahedra with four- and five-membered rings in the *ab* plane. **(b)** K, Ba, and REE cations distributing in channels along the *c* axis.

*Ima*2 and then to $P4/mbm$ upon heating, with $P4/mbm$ corresponding to the centrosymmetric high-temperature form and $P4bm$ to a polar lower-symmetry modification of the same framework. Xianhuaite-(Ce), with the ideal formula $K_2CeNb_5O_{15}$, is most directly comparable to synthetic $K_2CeNb_5O_{15}$, which is described in $P4/mbm$ at room temperature. Refinement of the present natural sample in $P4bm$ did not improve the model, giving $R1 = 0.0197$ compared with $R1 = 0.0189$ for $P4/mbm$. The intensity statistics also favor centrosymmetry, with a mean $|E^2 - 1|$ value of 0.925, closer to the expected value for centrosymmetric structures (0.968) than for non-centrosymmetric structures (0.736). Therefore, $P4/mbm$ is adopted as the room-temperature average structure of xianhuaite-(Ce).

Xianhuaite-(Ce) represents a new Nb mineral with a TTB-type structure, a structural topology not previously documented among natural Nb minerals. Its occurrence at Bayan Obo records a late-stage Nb reorganization process rather than primary Nb accumulation. The recognition of xianhuaite-(Ce) broadens the structural diversity of natural Nb minerals and provides additional constraints on Nb behavior during the multistage evolution of the Bayan Obo deposit.

Data availability. A CIF file is deposited in the Supplement section referred to below.

Supplement. The supplement related to this article is available online at https://doi.org/10.5194/ejm-38-449-2026-supplement.

Author contributions. BY found the mineral. BY, LY, XH, ZY, AX, and JW carried out fieldwork. GL, YX, and NS processed and interpreted the crystal structure data. ZC, ZL, JY, BY, and LC performed electron microprobe analysis. BY and YX drafted the paper. YZ, GY, JL, and WM supplied valuable critical insights that improved the paper's quality.

Competing interests. The contact author has declared that none of the authors has any competing interests.

Disclaimer. Publisher's note: Copernicus Publications remains neutral with regard to jurisdictional claims made in the text, published maps, institutional affiliations, or any other geographical representation in this paper. The authors bear the ultimate responsibil-

ity for providing appropriate place names. Views expressed in the text are those of the authors and do not necessarily reflect the views of the publisher.

Acknowledgements. We thank Xue Lou from the Instrumentation and Service Center for Molecular Sciences at Westlake University for assistance in measuring reflectance values and Xiaoguang Li for supporting the Raman analyses.

Financial support. This work was jointly supported by the National Natural Science Foundation of China (grant nos. 92262303 and 42302042); the Natural Science Foundation of Inner Mongolia Autonomous Region of China (grant nos. 2025QN04037 and 2025FX060); the Class A Project of Baotou Iron and Steel (Group) Co., Ltd. (grant no. BGKYKJ-ZY-2025-Z-01); the Baotou Municipal Science and Technology Bureau (grant no. 2023H1001); Baotou Iron and Steel (Group) Co., Ltd.; the Grassland Talents Program; the Technology Innovation Guidance Project of Inner Mongolia Autonomous Region; and the Fundamental Research Funds for the Central Universities (grant no. 2652022030).

Review statement. This paper was edited by Sergey Krivovichev and reviewed by three anonymous referees.

References

Amira, Y., Gagou, Y., Menny, A., Mezzane, D., Zegzouti, A., Elaatmani, M., and El Marssi, M.: Structural and Raman properties of the tetragonal tungsten bronze ferroelectric $Pb_{2(1-x)}K_{1+x}Gd_xNb_5O_{15}$, Solid State Commun., 150, 419–423, https://doi.org/10.1016/j.ssc.2009.12.004, 2010.

Chen, Q., Song, W. L., Xu, C., Xue, S. N., Xu, D. N., and Chen, B.: Mineralogical and geochemical study of Nb mineralization in the giant Bayan Obo deposit, Ore Geol. Rev., 184, 106771, https://doi.org/10.1016/j.oregeorev.2025.106771, 2025.

Dolomanov, O. V., Bourhis, L. J., Gildea, R. J., Howard, J. A. K., and Puschmann, H.: Olex2: a complete structure solution, refinement and analysis program, J. Appl. Crystallogr., 42, 339–341, https://doi.org/10.1107/s0021889808042726, 2010.

Gagné, O. C. and Hawthorne, F.C.: Comprehensive derivation of bond-valence parameters for ion pairs involving oxygen, Acta Crystallogr. B., 71, 562–578, https://doi.org/10.1107/S2052520615016297, 2015.

Huang, Y. S., Li, X. C., Xu, X. W., Li, Q. L., Guo, Q., Liu, Y., Tang, G. Q., Li, X. H., and Fan, H. R.: New discovery of the Early Paleozoic carbonatite in Bayan Obo (China): Insights into the giant REE accumulation, Ore Geol. Rev., 170, 106156, https://doi.org/10.1016/j.oregeorev.2024.106156, 2024.

Ilinca, G.: Charge distribution and bond valence sum analysis of sulfosalts: The ECoN21 computer program, Minerals, 12, 924, https://doi.org/10.3390/min12080924, 2022.

Institute of Geochemistry, Chinese Academy of Sciences: Geochemistry of the Bayan Obo ore deposit, Science Press, Beijing, 535 pp., ISBN 7–03–000317–9/P·50, 1988 (in Chinese).

Li, X. C., Fan, H. R., Su, J. H., Groves, D. I., Yang, K. F., and Zhao, X. F.: Giant rare earth element accumulation related to voluminous, highly evolved carbonatite: A microanalytical study of carbonate minerals from the Bayan Obo deposit, China, Econ. Geol., 119, 373–393, https://doi.org/10.5382/econgeo.5060, 2024.

Li, Y., Wu, L. G., Yu, Y., Yang, L., Selby, D., and Li, X. H.: Paleozoic carbonatites controlled rare-earth-elements mineralization at Bayan Obo, Sci. Adv., 11, eads9481, https://doi.org/10.1126/sciadv.ads9481, 2025.

Mandarino, J. A.: The Gladstone-Dale relationship: Part IV. The compatibility concept and its application, Can. Mineral., 19, 441–450, 1981.

Mazurov, M. P., Grishina, S. N., Titov, A. T., and Shikhova, A. V.: Evolution of ore-forming metasomatic processes at large skarn iron deposits related to the traps of the Siberian Platform, Petrology, 26, 265–279, https://doi.org/10.1134/s0869591118030049, 2018.

Momma, K. and Izumi, F.: VESTA 3 for three-dimensional visualization of crystal, volumetric and morphology data, J. Appl. Crystallogr., 44, 1272–1276, https://doi.org/10.1107/s0021889811038970, 2011.

Ren, Y. S., Yang, X. Y., Yang, X. M., and Liu, Y. L.: Mineralogical study on the distribution regularity of niobium in various types of ores in the giant Bayan Obo Fe-REE-Nb deposit, Ore Geol. Rev., 161, 105602, https://doi.org/10.1016/j.oregeorev.2023.105602, 2023.

Rooks, C. J., Finch, A. A., Hutchison, W., Herd, D. A., and Frangeskides, G.: Rare earth and niobium mobility at the magmatic-hydrothermal transition: Motzfeldt Sø Centre, Greenland, Ore Geol. Rev., 188, 107009, https://doi.org/10.1016/j.oregeorev.2025.107009, 2025.

She, H. D., Fan, H. R., Yang, K. F., Li, X. C., Yang, Z. F., Wang, Q. W., Zhang, L. F., and Wang, Z. J.: Complex, multi-stage mineralization processes in the giant Bayan Obo REE-Nb-Fe deposit, China, Ore Geol. Rev., 139, 104461, https://doi.org/10.1016/j.oregeorev.2021.104461, 2021.

Sheldrick, G. M.: Crystal structure refinement with SHELXL, Acta Crystallogr., C, 71, 3–8, https://doi.org/10.1107/S2053229614024218, 2015.

Tytko, K. H., Mehmke, J., and Kurad, D.: Bond length–bond valence relationships with particular reference to polyoxometalate chemistry, Struct. Bond., 93, 1–66, https://doi.org/10.1007/BFb0103378, 1999.

Yang, B., Yang, L., Zhao, Y. G., Yan, G. Y., Liu, J. Y., Meng, W. X., Yu, J. F., Chen, L., Li, X. X., and Li, X. H.: Aeschynite group minerals are a potential recovery target for niobium resources at the giant Bayan Obo Nb–REE–Fe deposit in China, Minerals, 14, 1029, https://doi.org/10.3390/min14101029, 2024a.

Yang, K. F., Fan, H. R., Pirajno, F., and Liu, X.: Magnesium isotope fractionation during differentiation of mafic-alkaline-carbonatitic magma and Fe-P-REE-rich melt at Bayan Obo, China, Ore Geol. Rev., 157, 105466, https://doi.org/10.1016/j.oregeorev.2023.105466, 2023.

Yang, L., Yan, G. Y., Yang, B., and Meng, W. X.: Bayan Obo minerals, Geological Publishing House, Beijing, 177 pp., ISBN 978-7-116-13744-8, 2024b (in Chinese).

Yang, L., Li, Y., Liu, Y., Ling, X. X., Wu, L. G., Yu, Y., Meng, W. X., Yan, G. Y., and Li, X. H.: Lead-lead dating reveals Permian

remobilization of niobium mineralization at Bayan Obo, Econ. Geol., 119, 1383–1391, https://doi.org/10.5382/econgeo.5096, 2024c.

Yao, L. H., Li, Y., Zhang, W., Yang, L., Yu, Y., and Yang, B.: Geochemical characteristics and *in situ* Rb-Sr dating of mica from the Bayan Obo deposit: implications for REE-Nb ore formation, Acta Petrol. Sin., 41, 1149–1169, https://doi.org/10.18654/1000-0569/2025.04.03, 2025 (in Chinese).

Yu, Y., Li, Y., Liu, Y., Ling, X. X., Wu, L. G., Yang, L., Yang, B., Zhao, Y. G., and Li, X. H.: Three-stage niobium mineralization at Bayan Obo, China, Natl. Sci. Rev., 11, nwae063, https://doi.org/10.1093/nsr/nwae063, 2024.

Zeng, Q., Ge, H., Wu, M. F., Ruan, S. H., Li, T. T., Wang, Z. S., Li, J. X., Ling, L. S., Tong, W., Huang, S., Liu, A., Zhou, J., Xia, Z. C., Sheng, J. M., Wu, L. S., and Tian, Z. M.: $K_2RENb_5O_{15}$ (RE = Ce, Pr, Nd, Sm, Gd−Ho): A Family of Quasi-One-Dimensional Spin-Chain Compounds with Large Interchain Distance, Chem. Mater., 36, 2867–2879, https://doi.org/10.1021/acs.chemmater.3c03217, 2024.